Macedonian Journal of Chemistry and Chemical Engineering, Vol. **44**, No. 1, pp. xx–xx (2025)

MJCCA9 –

ISSN 1857-5552
e-ISSN 1857-5625

Received: March 14, 2025
Accepted: April 14, 2025

DOI: 10.20450/mjcce.2025.3101
Original scientific paper

STRUCTURALLY ENGINEERED COBALT−IRON LAYERED DOUBLE HYDROXIDE ON METAL ORGANIC FRAMEWORK ELECTROCATALYST FOR ENHANCED ELECTROCATALYTIC WATER SPLITTING PERFORMANCE

Yasir Hashmi, Jianzhi Wang, Faquan Yu*

Key Laboratory for Green Chemical Process of Ministry of Education,
Hubei Key Laboratory for Novel Reactor and Green Chemistry Technology,
Hubei Engineering Research Center for Advanced Fine Chemicals,
School of Chemical Engineering and Pharmacy,
Wuhan Institute of Technology, Wuhan 430073, China
fyu@wit.edu.cn

Metal-organic frameworks (MOFs) have garnered significant attention as potential electrocatalysts. However, their direct application as bifunctional catalysts for overall water splitting remains challenging. In this study, we successfully synthesized a three-layered cobalt-iron layered double hydroxide (CoFe-LDH) on a MOF (CoFe-MOF) hybrid electrode (CoFe-LDH@CoFe-MOF/Co/CC) using a simple solvothermal method. Based on electrochemical analysis, this electrode exhibits remarkable electrocatalytic performance, requiring a low overpotential of 365 mV at 50 mA/cm^2 for the oxygen evolution reaction (OER). The outstanding catalytic performance is attributed to the unique hierarchical structure and the synergistic effect between CoFe-LDH and CoFe-MOF. Additionally, electrochemical testing suggests that other species formed during the reaction contribute to the enhanced activity of this material. Our findings offer valuable insights into the rational design of MOF-based electrocatalysts for efficient water splitting applications.

Keywords: electrocatalyst; MOFs; OER; solvothermal; synergistic effect

СТРУКТУРНО ДИЗАЈНИРАН ДВОЕН ХИДРОКСИДЕН СЛОЈ ОД КОБАЛТ-ЖЕЛЕЗО ВРЗ МЕТАЛ-ОРГАНСКА ЕЛЕКТРОКАТАЛИТИЧКА РАМКА ЗА ПОДОБРЕНИ ЕЛЕКТРОКАТАЛИТИЧКИ ПЕРФОРМАНСИ ЗА РАЗЛОЖУВАЊЕ НА ВОДА

Метал-органските структурни рамки (MOF) привлекуваат значително внимание како потенцијални електрокатализатори. Имено, нивната директна примена како бифункционални катализатори за целосно разложување на водата претставува предизвик. Во оваа студија е претставен протокол за синтеза на тросолен двоен хидроксид на база на кобалт-железо врз метал-органска структурна хибридна електрода (CoFe-LDH@CoFe-MOF/Co/CC) со примена на едноставен метод на термално растворање. Врз основа на резултатите добиени од електрохемисите анализи, оваа електрода покажува многу добри електрокаталитички перформанси, при што за реакцијата на еволуција на кислород е потребен мал наднапон од 365 mV при густина на струја од 50 mA/cm². Исклучителните катализаторски перформанси на дизајнираната хибридна електрода се базираат пред сè на уникатната хиерархиска структура и синергетскиот ефект помеѓу метално-органските слоеви CoFe-LDH и CoFe-MOF. Покрај тоа, електрохемиските испитувања сугерираат дека и други соединенија и структури, што се формираат за време на реакцијата на синтеза, придонесуваат за зголемената активност на овој материјал. Резултатите од овие студии претставуваат вреден придонес кон едноставен дизајн на електрокатализатори базирани на метал-органски рамки што би се употребиле за ефикасно разложување на вода.

Клучни зборови: електрокатализатори; метал-органски рамки; еволуција на кислород; термално растворање; синергетски ефект

1. INTRODUCTION

The increasing global energy demand and environmental concerns have intensified the search for sustainable energy sources.[1,2] Among various approaches, electrochemical water splitting is a promising method for producing high-purity hydrogen and oxygen, involving the hydrogen evolution reaction (HER) at the cathode and the oxygen evolution reaction (OER) at the anode.[3,4] In this process, a water molecule is split into hydrogen and oxygen under an applied potential of 1.23 V. However, practical implementation of OER poses challenges, requiring a higher potential than the theoretical value.[5] This is attributed to the inherently sluggish nature of the four-electron-associated multistep OER, in contrast to the more efficient two-electron transfer in the HER.[6] Compounding these challenges, the most advanced OER catalysts currently rely on expensive and scarce precious metals such as ruthenium (Ru) and iridium (Ir), which greatly limits their widespread commercial applications. It is highly desirable to develop low-cost transition metal alternatives that display comparable OER kinetics and have progressed significantly in recent years.[7–9]

To achieve high catalytic activity, micro/nanostructured catalysts with porous properties are an important way to expose active sites as much as possible to the electrolyte and substrate. There has been increased interest in the metal-organic framework (MOF), which derives from the variety and designability of compositions and structures, in the fields of material science, chemical engineering, and chemistry. When utilized as nano-catalysts, they show remarkable efficiency owing to their open active sites and minimized mass transfer resistance facilitated by their inherent hierarchical porosity.[10] Certain MOFs based on transition metals, including nickel (Ni)-MOF, cobalt (Co)-MOF, and cobalt iron (CoFe)-MOF, have recently been discovered to have potential uses in energy-related domains,[11–13] taking advantage of their wide surface areas, porous nature, varied functional groups and metallic centers, and evenly dispersed activated metal sites.[14,15] However, direct application of MOFs in electrocatalytic domains, such as water splitting, is hampered by their intrinsic constraints, which include low electrical conductivity, limited mass permeability, and difficulties in controlling morphology.[16,17] The micro/nanostructures of MOFs are frequently used as precursors in the pyrolysis or chemical reactions used to synthesize different metal compound catalysts in order to increase electrocatalytic activity.[18,19] Nevertheless, a major obstacle still stands in how to use pure MOF-based micro/nanostructures as effective bifunctional electrocatalysts for total water splitting.[20,21]

An improvement in performance entails adding more metal components, combining conductive substrates, or optimizing the structure.[17,18,22] Given that 0 D single metal nanoparticles and 2D metal layered double hydroxide (LDH) nanosheets are excellent conductors, the formation of hybrid structures between the MOF nanocomposites and single metal nanoparticles and 2D metal LDH nanosheets might effectively exert their synergistic effect by taking advantage of their respective advantages. In this study, we designed a structurally engineered sunflower-like CoFe-LDH@CoFe-MOF/Co/CC electrocatalyst via a controlled solvothermal synthesis. The introduction of an LDH enhances charge transport, while the integration of MOFs provides abundant active sites. The optimized hybrid structure significantly improves catalytic activity, achieving a low overpotential of 365 mV at 50 mA/cm^2.

2. EXPERIMENTAL SECTION

2.1. *Materials and reagents*

Cobalt chloride hexahydrate ($CoCl_2 \cdot 6H_2O$, 99.5 %), ethanol (CH_3CH_2OH, 99.7 %), ferric chloride ($FeCl_3 \cdot 6H_2O$, 99.5 %), potassium hydroxide (KOH), and *N*,*N*-dimethyl formamide (DMF, 99.5 %) were purchased from Sino Pharm Chemical Reagent Co, Ltd. (China). Carbon cloth (CC) was purchased from DuPont China Holding Co., Ltd. (China). Hydrochloric acid (HCl) and 2,5-dihydroxyterephthalic acid ($C_8H_6O_6$, 98 %) was obtained from China. All chemical reagents were of analytical grade and used without any further purification. Experiments used only deionized water.

2.2. *Synthesis of Co/CC*

In the first step, a CC was cleaned and washed ultrasonically to remove contaminants on the surface with deionized water for 10 min, 3 mol of HCl for 30 min, and ethanol for 10 min. Then, it was rinsed in deionized water for subsequent use.[23] A solution was prepared by mixing 1 mmol of $CoCl_2 \cdot 6H_2O$ in 7 ml of deionized water, 7 ml of ethanol, and 7 ml of DMF. The solution and a piece of CC were placed in a glass vial, and the vial was placed in a 100-ml teflon-lined hydrothermal autoclave and heated in a furnace at 120°C for 6 h.[24] After freeze drying, the as-obtained

Co/CC was cleaned with deionized water and ethanol several times and reserved for use in the next reaction.[25]

2.3. *Synthesis of CoFe-MOF/Co/CC*

One millimole of $CoCl_2 \cdot 6H_2O$, 1 millimole of $FeCl_3 \cdot 6H_2O$, and 1 millimole of 2,5-dihydroxyterphthalic acid were dissolved in a mixture of 7 ml of deionized water, 7 ml of ethanol, and 7 ml of DMF. The obtained solution and a piece of Co/CC was transferred to a vial. Then, the vial was placed in a 100-ml teflon-lined hydrothermal autoclave and heated in furnace at 120°C for 6 h. Finally, CoFe-MOF/Co/CC was obtained and rinsed with water. For comparison, CoFe-MOF/CC was also produced via a similar procedure used to synthesize CoFe-MOF/Co/CC, except CC was used instead of Co/CC.

2.4. *Synthesis of CoFe-LDH@CoFe-MOF/Co/CC*

One millimole of $CoCl_2 \cdot 6H_2O$ and 1 mmol of $FeCl_3 \cdot 6H_2O$ were dissolved in a mixture of 7 ml of deionized water, 7 ml of ethanol, and 7 ml of DMF. The obtained solution and a piece of CoFe-MOF/Co/CC were transferred to a vial. Then, the vial was placed in a 100-ml teflon-lined hydrothermal autoclave and heated in furnace at 120 °C for 6 h. Finally, CoFe-LDH@CoFe-MOF/Co/CC was obtained and rinsed with water.

2.5. *Synthesis of CoFe-LDH Co/CC and CoFe-LDH CoFe-MOF/CC*

CoFe-LDH Co/CC and CoFe-LDH CoFe-MOF/CC were synthesized via the same method as that for CoFe-LDH@CoFe-MOF/Co/CC, except Co/CC and CoFe-MOF/CC was used instead of CoFe-MOF/Co/CC, respectively.

2.6. *Material characterization*

X-ray powder diffraction (XRD) patterns were examined by using Cu-K radiation at a scanning rate of 2°/min in the 2θ range from 5° to 90° on a D8 Advance (Brucker AXS, Germany). X-ray photoelectron spectroscopy (XPS) was carried out on an ESCLAB 250Xi spectrophotometer (Thermo Fisher Scientific, USA) to analyze the valence state. XPS spectra were referenced to the C 1s peak of 284.8 eV. The morphology was characterized by field emission scanning electron microscopy (FESEM, Gemini SEM 300, Carl Zeiss, Germany) and energy dispersive spectroscopy (EDS) mapping. Transmission electron microscopy (TEM) images were obtained with a JEM 2100 (JEOL Ltd., Japan), which also provided information on lattice fringe.

2.7. *Electrochemical measurements*

The electrochemical test results were obtained with a CHI 760 electrochemical workstation (CHI Instruments, Shanghai Chenhua Instrument Corp., China) in a standard three-electrode system at room temperature. The as-prepared catalysts, Hg/HgO electrode, and graphite rod were used as the working, reference, and counter electrodes, respectively. In all measurements, the potentials were calculated with respect to reversible hydrogen electrode (RHE) based on the following equation:

$$E(\text{RHE}) = E(\text{SCE}) + 0.059 \times \text{pH} + 0.242 \text{ V}$$

Linear sweep voltammetry (LSV) curves were generated in 1 M KOH (as an electrolyte) with a scan rate of 2 mV/s; they were generated after 20 cycles of cyclic voltammetry (CV) to stabilize the current. All polarization potentials were calibrated with 85% iR compensation. CV curves with different scan rates (10–100 mV/s) were determined over a potential range in which redox processes were absent to calculate the electrochemical double-layer capacitance:

$$C_{dl} = \frac{(ja - jc)}{2v} = \frac{(ja + |jc|)}{2v} = \frac{\Delta j}{2v}$$

where C_{dl} is the double-layer capacitance of the electroactive materials, and *ja* and *jc* are the anodic and cathodic current density (mA/cm), respectively, recorded at the middle of the selected potential range, and *v* is the scan rate (mV/s). Electrochemical impedance spectroscopy (EIS) was operated on the same standard three-electrode glass cell system in a 1 M KOH electrolyte with a frequency range of 0.01–100 kHz and an amplitude of 5 mV. Cycling stability was tested by observing the LSV polarization curve before and after 1,000 continuous CV cycles at a scan rate of 100 mV/s. Long-term stability was evaluated using chronopotentiometry at a constant current density of 10 mA/cm.

3. RESULTS AND DISCUSSION

In Scheme 1, the schematic representation of the synthesis process is shown, detailing the steps involved in the preparation of the CoFe-LDH@CoFe-MOF/Co/CC electrode. Following the electrochemical deposition of metallic Co,

SEM analysis revealed features consistent with the presence of nanoparticles on the CC surface (Co/CC). Then, in the presence of the ligand 2,5-dihydroxyterephthalic acid, Co^{2+} generated *in situ* under solvothermal conditions combines with the ligand to form CoFe-MOF, which subsequently attaches to the Co/CC surface (CoFe-MOF@Co/CC, Fig. S1). This attachment process is crucial because it facilitates the integration of the CoFe-MOF complex onto the conductive CC substrate, establishing a robust interface. The LDH can be introduced between the CoFe-MOF and Co/CC supports. It can act as a binder, further strengthening the attachment between the CoFe-MOF and the CC. This improved interface can lead to better stability and durability of the overall material. The CoFe-LDH@CoFe-MOF/Co/CC hybrid material holds promise for various applications due to its unique combination of properties. The conductivity of the CC substrate enhances electron transfer, while the CoFe-MOF provides catalytic activity and selectivity. This synergistic effect opens avenues for diverse applications, including energy conversion and storage, electrocatalysis, and environmental remediation. Moreover, the controlled synthesis of the CoFe-LDH@CoFe-MOF/Co/CC hybrid material allows for tunability of its properties, further expanding its potential applications in advanced technologies.

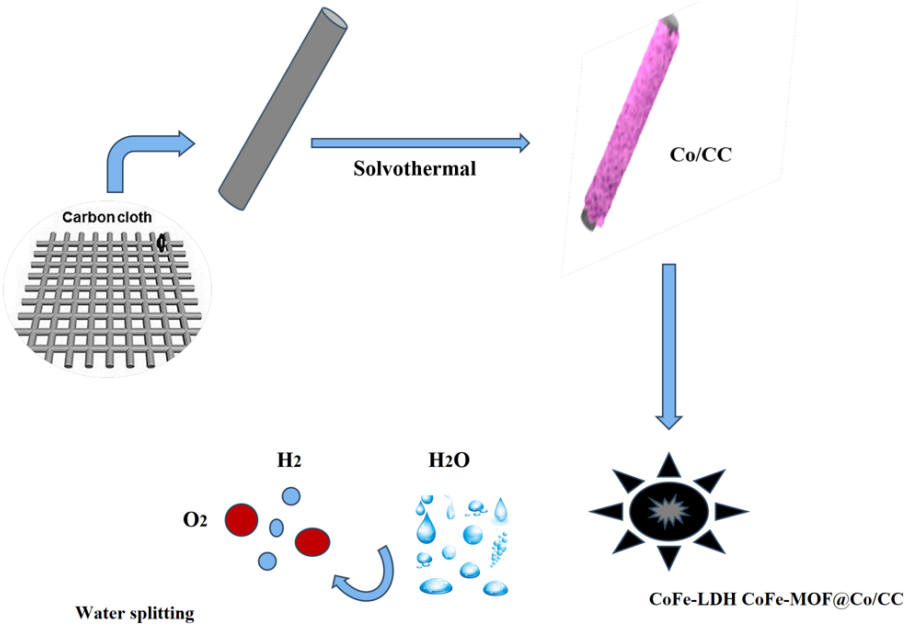

Scheme 1. Schematic of the synthesis of the CoFe-LDH CoFe-MOF@Co/CC nanoarrays for water splitting

The high-resolution SEM images (Fig. 1a–f) show the CoFe-LDH@CoFe-MOF nanoparticles anchored on the CC substrate. Notably, these nanoparticles possess an intriguing sunflower-like morphology, characterized by a central core and branching structures. This unique architecture could potentially offer a high surface area, which might be beneficial for the desired electrocatalytic activity.[26] For comparison, the microstructures of CoFe-LDH@Co/CC and CoFe-LDH@CoFe-MOF /CC were also examined, as shown in Figs. S2 and S3. In Fig. S2, the SEM images of the CoFe-LDH@Co/CC at various magnifications show the detailed morphology—flower-like, sheet-like nanostructures of the material, highlighting the nanoscale features and structure of the composite. CoFe-LDH nanostructures are integrated onto Co/CC, which serves as the conductive support. In Fig. S3, the SEM images of CoFe-LDH@CoFe-MOF/CC at different magnifications reveal the nanostructure of the composite, emphasizing the integration of CoFe-LDH and CoFe-MOF on the conductive substrate. Elemental distribution analysis via EDS mapping (Fig. 1g) confirmed the homogeneous dispersion of Co, Fe, oxygen (O), and carbon (C) throughout the composite, validating its compositional uniformity. The presence of O suggests the formation of hydroxides/oxides, which play a key role in electrocatalysis.

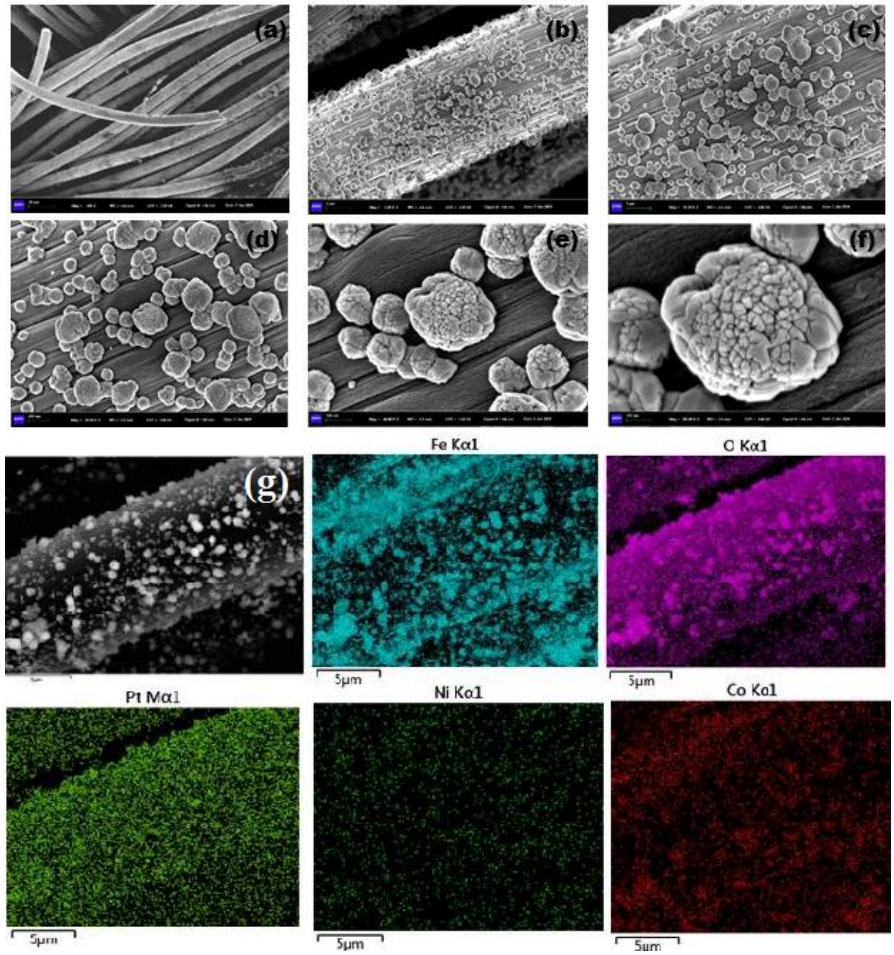

Fig. 1. (a–f) FESEM images of CoFe-LDH@CoFe-MOF@Co/CC. (g) SEM-EDS mapping images of CoFe-LDH@CoFe-MOF@Co/CC

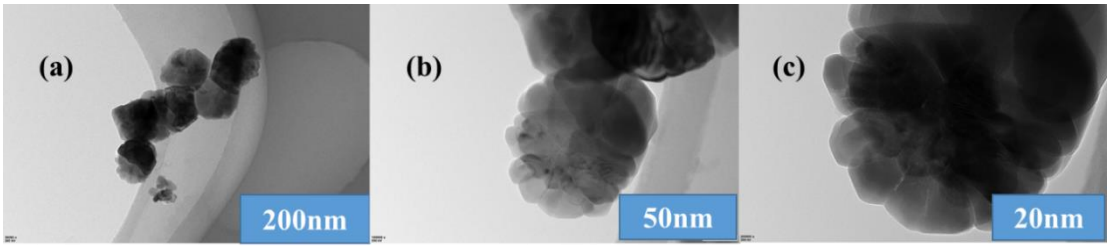

Fig. 2. (a) TEM and (b, c) high-resolution TEM images of CoFe-LDH@CoFe-MOF@Co/CC

The structure and chemical composition of the CoFe-LDH@CoFe-MOF@/Co/CC electrode were analyzed with TEM. Co/CC is composed of a large number of nanoparticles with a diameter of approximately 50 nm (Fig. 2a). As shown in Figures 2b and 2c, high-resolution TEM imaging further indicates that small particles with diameters ranging from 15 to 22 nm are uniformly distributed around the periphery of each nanoparticle. Thus, binding of the CoFe-MOF and the CoFe-LDH leads to better charge transfer and more exposed active sites. This synergistic effect enhances the kinetics of the OER and reduces the required overpotential.

Figure 3 shows the XRD patterns of products obtained at various stages. Co/CC exhibits a strong, broad peak in the 20°–30° range, attributed to C, and weak peaks in the 40°–50° range due to Co (PDF # 01-1277). These XRD results confirm successful Co loading onto the CC. The first peak at 34.4° is due to the decomposition of the Co oxides produced during the reaction in the autoclave at a high temperature into Co and O. Following solvothermal treatment in ligand and H^+/Fe^{3+} ion

systems, Co diffraction peaks remain detectable albeit with reduced intensities, indicating the presence of metallic Co post-MOF formation. This achievement is crucial for creating a composite material with enhanced properties and functionalities, as metallic Co serves as an active component in various catalytic and electrochemical applications. Although the diffraction peaks corresponding to Co exhibit reduced intensities, they remain detectable even after formation of the MOF. The persistence of the Co diffraction peaks post-MOF formation suggests that Co is retained within the composite material, albeit potentially in a modified state. This observation underscores the robustness of the metallic Co/CC system and its ability to withstand solvothermal treatment without complete transformation or degradation. The reduction in the intensity of Co diffraction peaks may be attributed to various factors, including the incorporation of Co ions into the MOF structure, changes in crystallinity, or surface interactions between Co and other species present in the system.

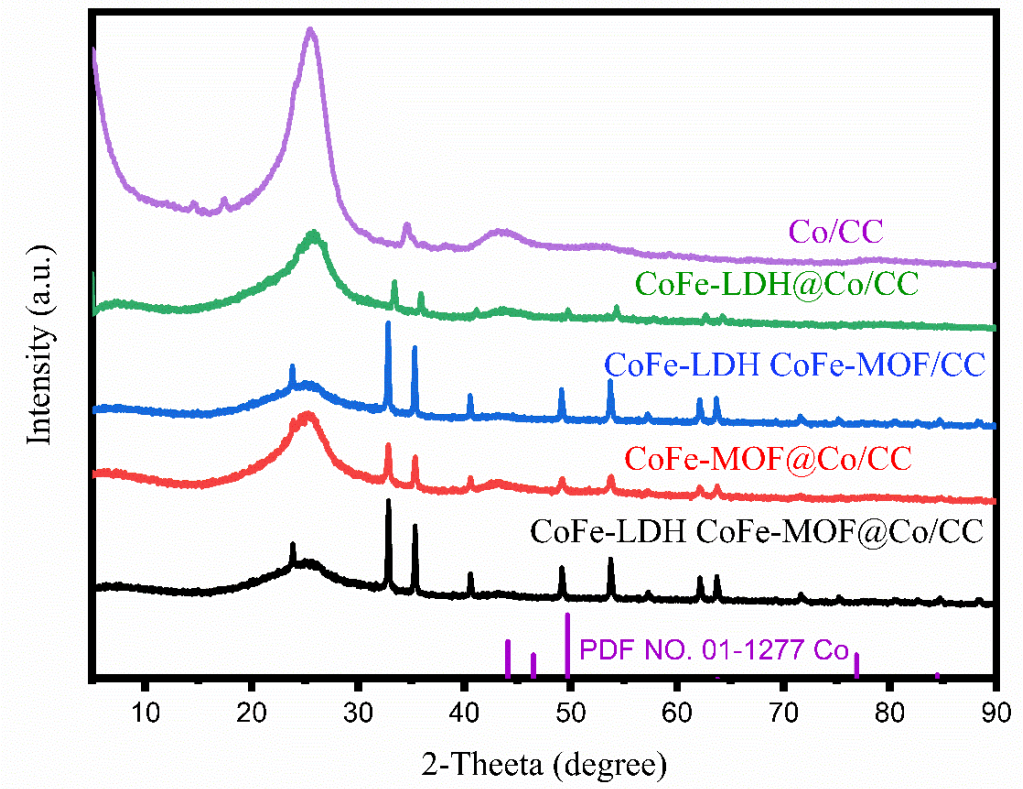

Fig. 3. XRD patterns of Co/CC, CoFe-LDH@Co/CC, CoFe-LDH CoFe-MOF/CC, CoFe-MOF@Co/CC, and CoFe-LDH CoFe-MOF@Co/CC

The successful introduction of Fe into the Co-MOF was validated through XPS analyses. Fig. 4a shows the survey spectrum of CoFe-MOF/CC, which contains the elements Co, Fe, O, and C. The high-resolution XPS spectrum of Fe 2p (Fig. 4b) presents two peaks centered at 711.2 and 723.4 eV, along with corresponding satellite peaks at 709.1 and 724.1 eV, attributed to Fe^{2+}.[27] This confirms the presence of Fe^{2+} in CoFe-LDH CoFe-MOF/CC. Furthermore, the successful integration of Fe into Co-MOF/Co/CC led to a change in the binding energy of Co 2p. As shown in Fig. 4c, the Co 2p1/2 peak is located at 786.46 eV in the CoFe-LDH CoFe-MOF/CC, while after the formation of CoFe-LDH CoFe-MOF/CC, it shifts to 782.11 eV. This indicates a 4.35 eV decrease in binding energy, signifying an increase in electron density at the Co center following Fe doping. Of note, the Co center with an electron-rich structure favors the formation of key intermediates, such as hydroperoxy (•OOH) species, which enhance OER activity.[11,28]

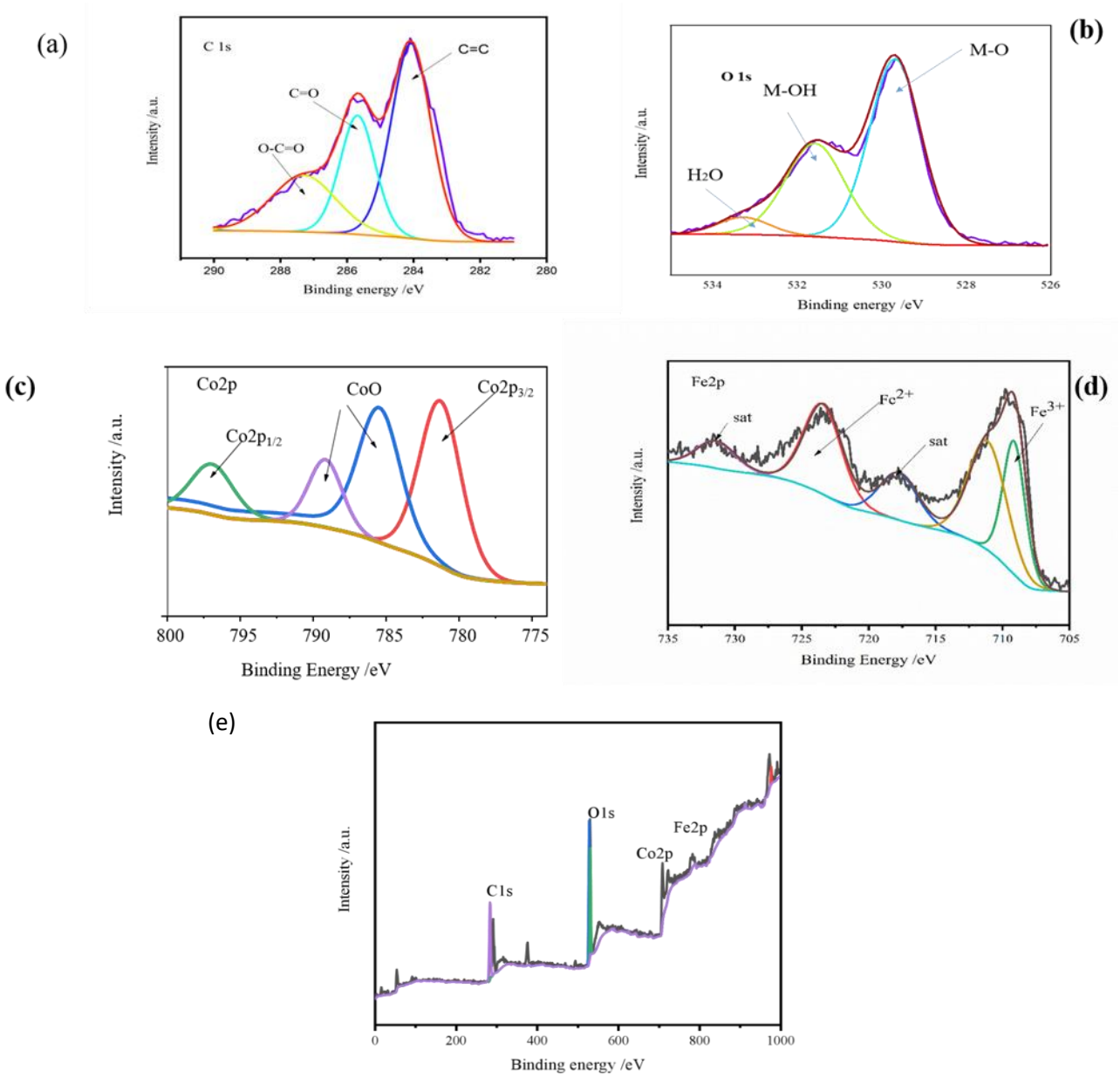

Fig. 4. High-resolution XPS spectra of (a) C1s, (b) O1s, (c) Co 2p, and (d) Fe 2p for CoFe-LDH@CoFe-MOF@/Co/CC. (e) XPS survey spectra of CoFe-LDH@CoFe-MOF@/Co/CC

The electrocatalytic activities of the samples toward the OER were measured in 1.0 M KOH (which served as the electrolyte) by using a three-electrode configuration. Figure 5a depicts the LSV curves for the commercial Co/CC, CoFe-LDH@CoFe-MOF/CC, and CoFe-LDH CoFe-MOF@/Co/CC electrodes during the OER. At a current density of 50 mA/cm^2, the resulting electrode requires only 365 mV of overpotential, surpassing the overpotential of 365 mV for CoFe-LDH@/CoFe-MOF/Co/CC, 389 mV for CoFe-LDH@/Co/CC, 414 mV for Co/CC, and 401 mV for CoFe-MOF@Co/CC. Co/CC was synthesized through a straightforward solvothermal method. Subsequently, Co/CC was employed as a substrate for the growth of an MOF, resulting in CoFe-MOF@Co/CC. This MOF formation was facilitated by another solvothermal process that utilized equal volumes of three solvents and the linker molecule 2,5-dihydroxyterephthalic acid. The linker coordinates with Co metal centers, enhancing the catalyst's efficiency for the OER. Finally, the introduction of LDH onto pre-synthesized CoFe-MOF@Co/CC via an additional step yielded the final, functional electrocatalyst: CoFe-LDH@Co Fe-MOF@Co/CC. The integration of CoFe-LDH @CoFe-MOF on the Co/CC substrate stands out as a pivotal factor in augmenting the electrocatalytic

activity of the catalyst. The synergistic effect of Co and Fe within the hybrid structure further amplifies the efficiency of the catalyst, resulting in superior performance metrics compared with other configurations. These findings highlight the potential of tailored catalyst compositions, such as CoFe-LDH CoFe-MOF@/Co/CC, in advancing the efficacy of electrocatalytic systems for various applications, including energy conversion and storage. Moreover, the observed overpotential exceeds what has been reported for the majority of Co- and Fe-based electrocatalysts in the literature, underscoring the exceptional performance of the CoFe-LDH CoFe-MOF@/Co/CC catalyst.[29]

Particularly noteworthy is the superior catalytic activity of the CoFe-LDH CoFe-MOF@/Co/CC electrode, indicating that incorporating the appropriate amount of Fe further enhances the performance of catalysts. We used 1 mM of Fe in our solution while preparing CoFe-LDH CoFe-MOF@/Co/CC catalyst.

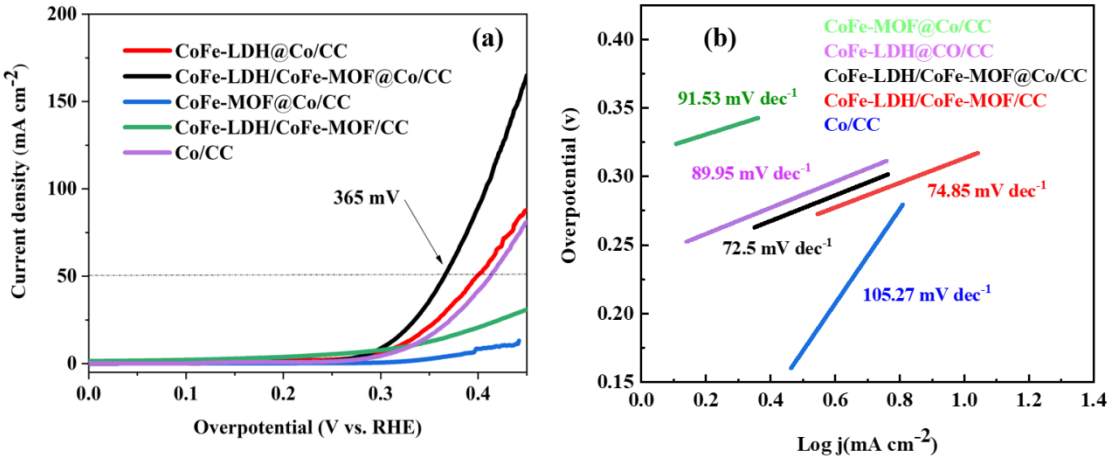

Fig. 5. (a) LSV curves and (b) the corresponding Tafel slopes of the Co/CC, CoFe-LDH CoFe-MOF/CC, CoFe-LDH CoFe-MOF@Co/CC, CoFe-LDH@Co/CC and CoFe-MOF@Co/CC electrodes in 1 M KOH (as the electrolyte) for the OER

In electrochemical reactions, the connection between the current density and the overpotential — that is, the discrepancy between the thermodynamic potential and the actual potential — is characterized by a parameter known as the Tafel slope,[30,31] which connects the overpotential to the rate of an electrochemical reaction. A lower Tafel slope suggests a faster reaction rate and more effective electrochemical kinetics by showing a faster rise in current density with increasing overpotential.[32] As shown in Figure 5b, the Tafel slope for each electrode is as follows: 91.53 mV/dec for CoFe-MOF@/Co/CC, 89.95 mV/dec for CoFe-LDH@/Co/CC, 74.85 mV/dec for CoFe-LDH CoFe-MOF/CC, 72.5 mV/dec for CoFe-LDH CoFe-MOF@/Co/CC, and 105.27 mV/dec for Co/CC. The CoFe-LDH CoFe-MOF@/Co/CC catalyst exhibits the smallest Tafel slope among the investigated catalysts, reflecting highly favorable catalytic kinetics and affirming its potential as an efficient electrocatalyst for water splitting applications. Figure 6 presents the cyclic voltammetry (CV) curves of various electrode configurations, including CoFe-MOF@/Co/CC, CoFe LDH@/Co/CC, CoFe-LDH CoFe-MOF/CC, CoFe-LDH@ CoFe-MOF@/Co/CC, and Co/CC electrodes, measured at different scan rates. The figure shows how the electrochemical activity of these electrodes varies with scan rate, which helps assess the electrochemical surface properties and the performance of each electrocatalyst for the oxygen evolution reaction (OER).

The electrochemical active surface area (ECSA) of the catalysts was determined through CV measurements. These measurements were carried out in a 1 M NaOH aqueous solution across a range of potential scan rates, typically ranging from approximately 20 to 100 mV/s, with potential variations spanning from 0.15 to 0.45 V versus the RHE, as demonstrated in Figure 7. These systematic CV analyses allowed for the ECSA of the catalysts to be quantified effectively, providing valuable insights into their electrochemical performance and surface characteristics. The CV curves exhibit a pseudo rectangular shape, devoid of discernible Faradic processes.[33] A higher value implies the presence of a larger number of exposed active sites, which facilitates and promotes various electrochemical processes. Consequently, this heightened accessibility to active sites enhances the efficiency and effectiveness of electrochemical reactions.

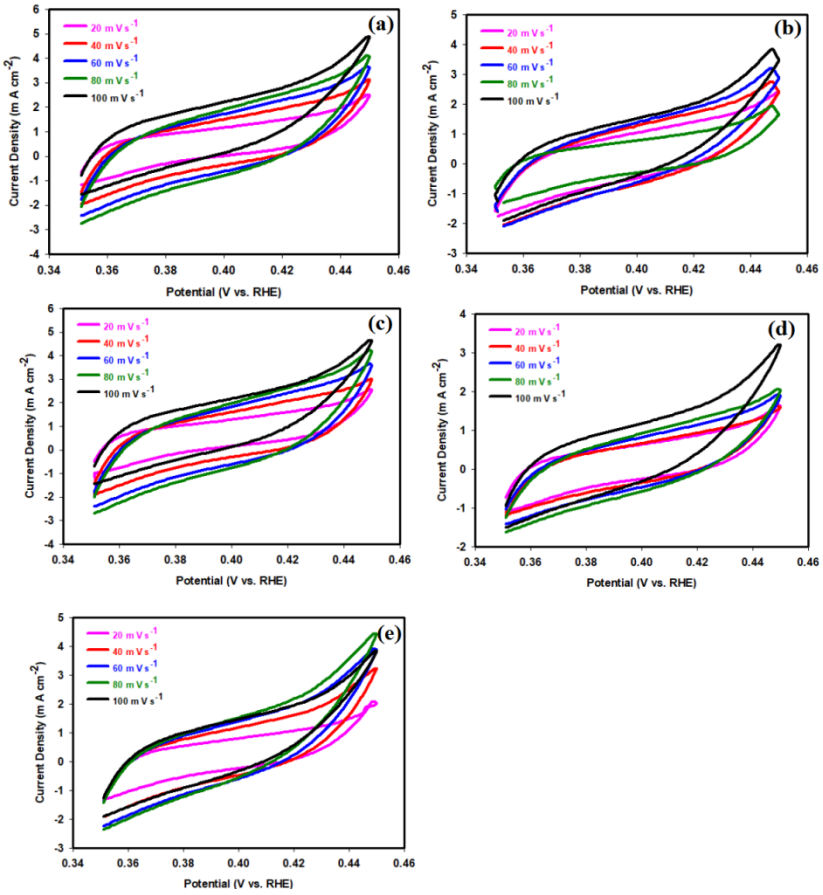

Fig. 6. CV curves of the (a) CoFe-MOF@/Co/CC, (b) CoFe-LDH@/Co/CC, (c) CoFe-LDH CoFe-MOF/CC, (d) CoFe-LDH@CoFe-MOF@/Co/CC and (e) Co/CC electrodes at different scan rates

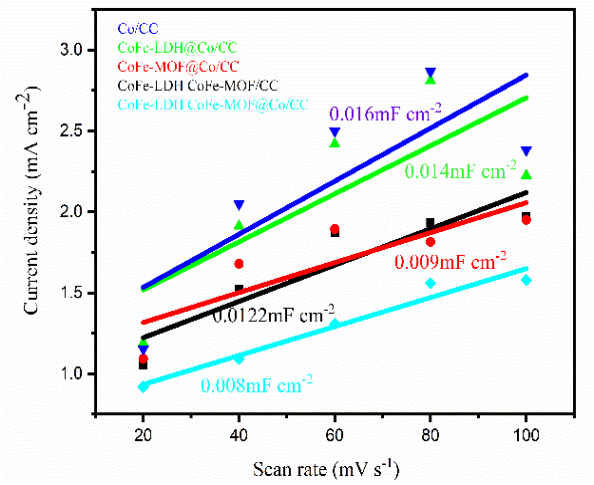

Fig. 7. The C_{dl} of the catalysts obtained from the current density curves obtained at different scan rates

Figure S4 represents the CV curves of various electrodes at a scan rate of 20, 40, 60, 80 and 100 mV/s. At the same scan rate, obviously, CoFe-LDH@CoFe-MOF@Co/CC presents the largest current density. Because the slope of the line equals twice the value of the double-layer capacitance (C_{dl}), the C_{dl} is 0.016 m F/cm^2 for Co/CC, 0.014 mF/cm^2 for CoFe-LDH@Co/CC, 0.009 mF/cm^2 for CoFe-MOF@/Co/CC, 0.0122 mF/cm^2 for CoFe-LDH CoFe-MOF/CC, and 0.008 mF/cm^2 for CoFe-LDH@CoFe-MOF@Co/CC. CoFe-LDH @CoFe-MOF@Co/CC has the largest C_{dl}. Because ECSA is proportional to C_{dl}, CoFe-LDH@CoFe-MOF@Co/CC also has the largest ECSA, demon-

strating that successful construction of CoFe-LDH@CoFe-MOF@Co/CC produces more ion-accessible sites for the OER. Obviously, CoFe-LDH@CoFe-MOF@Co/CC has the smallest charge-transfer resistance (R_{ct}) and the largest ECSA, which endows the best OER electrocatalytic performance. This suggests that CoFe-LDH CoFe-MOF@/Co/CC possesses a more favorable surface morphology and composition for catalytic activity, making it a promising candidate for applications requiring enhanced electrochemical performance.

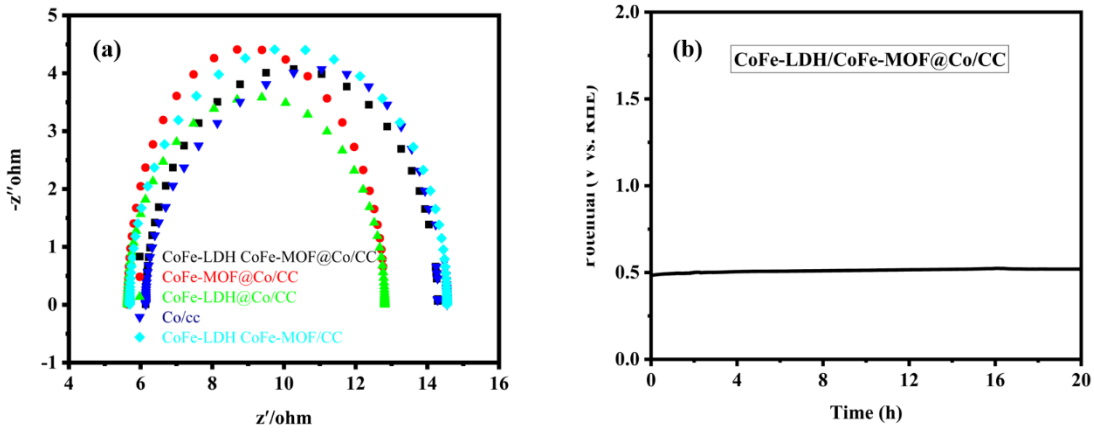

Fig. 8. (a) EIS spectra of CoFe-LDH@CoFe-MOF@/Co/CC, CoFe-MOF@/Co/CC, CoFe-LDH@/Co/CC, and Co/CC toward OER. (b) Static stability curve of CoFe-LDH@CoFe-MOF@/Co/CC

Figure 8a presents the Nyquist plots of various electrodes during the OER at 0.53 V, offering a comprehensive view of the mass transfer and charge transfer kinetics of the electrocatalyst. Notably, the CoFe-LDH@CoFe-MOF@/Co/CC electrode stands out with its remarkably low R_{ct} compared with the other electrodes. This observation suggests that there is an exceptionally rapid exchange of charges and surface reactions at the interface between the electrode and the electrolyte. The reduced R_{ct} underscores the efficient electron transfer processes and heightened catalytic activity of the CoFe-LDH CoFe-MOF@/Co/CC electrode, indicating its potential for enhanced performance in electrochemical applications. Figure 8b presents the chronopotentiometry curve of the CoFe-LDH @CoFe-MOF@/Co/CC electrode at a current density of 10 mA/cm^2. Impressively, even after continuous catalysis for 20 h, there was only a marginal increase in overpotential (35 mV). These results underscore the exceptional durability and cycle stability of the CoFe-LDH CoFe-MOF@/Co/CC catalyst for the OER.

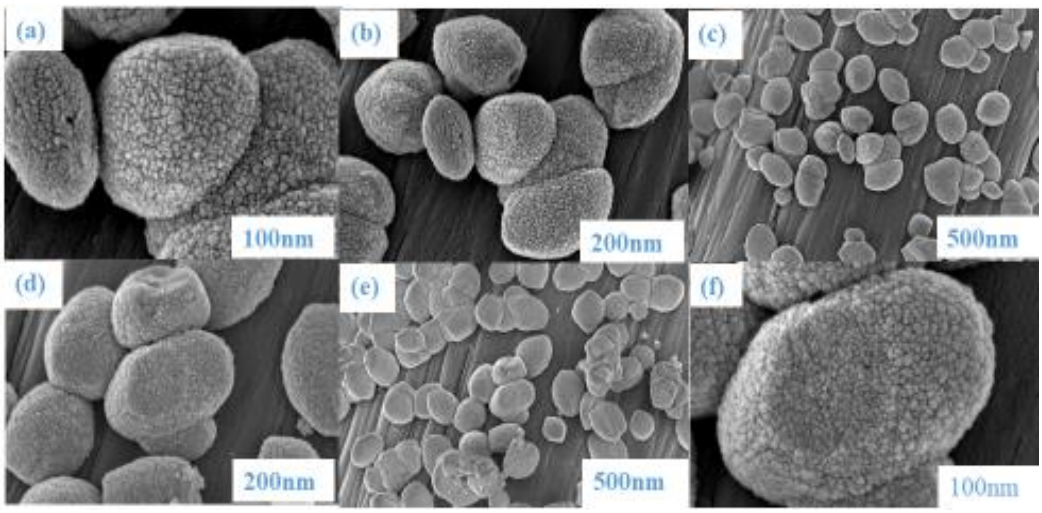

Fig. 9. (a–f) FESEM images of CoFe-LDH@CoFe-MOF@/Co/CC after 1000 CV cycles

Further investigation showed that during the OER, CoFe-LDH CoFe-MOF@Co/CC have different morphology and component change (Fig. 9). After 1000 CV cycles at the potential window of 0.35–0.45 V (vs. the RHE), the morphology of the catalyst changed from a sunflower-like structure to a small-ball-like structure. The XRD analysis proved that the CoFe-LDH@CoFe-MOF@Co/CC catalyst changes to metal oxyhydroxides, which is useful for OER. XRD analysis clearly showed that some peaks of CoFe-LDH@CoFe-MOF@Co/CC appear, which proves the presence of CoOOH. Oxyhydroxides formed *in situ* during electrochemical test act as active species for the OER. Fig. S6 shows a comparison of Co 2p XPS changes before and after CV activation. There are Co 2p peaks at ∼781.1 eV (2p3/2) and ∼797.2 eV (2p1/2) before CV activation. The XPS spin coupling orbit value of Co 2p is 16.1 eV, which is characteristic of Co^{2+}. After CV activation, the peaks at ∼779.6 eV (Co 2p3/2) and ∼794.7 eV (Co 2p1/2) with the XPS spin-orbit coupling value of ∼15.1 eV are ascribed to Co^{3+}. There are two new peaks at 712.5 and 726.1 eV in the Fe 2p XPS spectrum after CV activation (Fig. S6d), which are attributed to Fe^{3+}. Simultaneously, the electronic structure of O 1s in CoFe-LDH@CoFe-MOF@Co/CC also obviously changes before and after CV activation. The peaks at 531.5 and 533.5 eV are generated from M-O-R and O=C-O of the MOF, respectively. After activation, three peaks could be fitted. The peaks at 529.5 and 531.1 eV are due to presence of M-O and –OH group and the other peak may be due to presence of water molecules. Taken together, the data show that CoFe-LDH@CoFe-MOF@Co/CC is converted into CoOOH when the catalyst is activated. As a result, the CoOOH produced *in situ* acts as the electrocatalyst for the OER.

4. CONCLUSION

In this study, three-layered CoFe-LDH@ CoFe-MOF@Co/CC was synthesized via a straightforward solvothermal approach and evaluated systematically for its electrocatalytic activity toward the OER. The three-layered sunflower-like architecture provides a high surface area, allowing for a more effective interaction with the electrolyte, while the incorporation of LDH enhances the electrical conductivity and structural integrity of the catalyst. The CoFe-LDH@CoFe-MOF@ Co/CC catalyst delivers exceptional OER performance, achieving a low overpotential of 365 mV at 50 mA/cm^2 with a Tafel slope of 72.5 mV/dec. Remarkably, it maintains stable operation for 20 h with negligible overpotential degradation (<5% increase), demonstrating both high activity and durability. The MOF-on-LDH synthetic approach demonstrates excellent compatibility with various non-precious metal systems, offering a universal strategy for developing cost-effective, high-performance electrocatalysts. This work establishes a new paradigm for designing economically viable energy materials.

REFERENCES

(1) Lior, N., Sustainable energy development: the present (2009) situation and possible paths to the future. *Energy*, **2010**, *35* (10), p. 3976–3994. https://doi.org/10.1021/acsaem.8b02010

(2) Chu, S. and A. Majumdar, Opportunities and challenges for a sustainable energy future. *Nature*, **2012**, *488* (7411), p. 294–303. https://doi.org/10.1038/nature11475

(3) Tanveer ul Haq, T. and Y. Haik, *Electrochemical Water Splitting.* https://doi.org/10.1007/978-981-99-9860-9

(4) Hu, Q., *et al*., Recent progress in the hybrids of transition metals/carbon for electrochemical water splitting. *Journal of Materials Chemistry* A, **2019**, ***7*** (24), p. 14380-14390. https://doi.org/10.1039/C9TA04163J

(5) McHugh, P. J.; Stergiou, A. D.; Symes, M. D., Decoupled electrochemical water splitting: from fundamentals to applications. *Advanced Energy Materials*, **2020**, *10* (44), p. 2002453. (https://doi.org/10.1002/aenm.202002453)

(6) Govind Rajan, A.; Martirez, J. M. P.; Carter, E. A., Why do we use the materials and operating conditions we use for heterogeneous (photo) electrochemical water splitting? *ACS Catalysis*, **2020**, *10* (19), p. 11177–11234. https://doi.org/10.1021/acscatal.0c01862

(7) Solanki, R. *et al.*, Investigation of recent progress in metal-based materials as catalysts toward electrochemical water splitting. *Journal of Environmental Chemical Engineering*, **2022**, *10* (4), p. 108207. https://doi.org/10.1016/j.jece.2022.108207

(8) Ibrahim, K.B., *et al*., A review of transition metal-based bifunctional oxygen electrocatalysts. *Journal of the Chinese Chemical Society*, **2019**, *66* (8), p. 829–865. https://doi.org/10.1002/jccs.201900001

(9) Liu, Y., *et al*., Recent advances in carbon-supported noble-metal electrocatalysts for hydrogen evolution reaction: syntheses, structures, and properties. *Advanced Energy Materials*, **2022**, *12* (28), p. 2200928. https://doi.org/10.1002/aenm.202200928

(10) Wu, W., Jiang, C. Z.; Roy, V. A., Designed synthesis and surface engineering strategies of magnetic iron oxide nanoparticles for biomedical applications. *Nanoscale*, **2016**, *8* (47), p. 19421–19474. https://doi.org/10.1039/C6NR07542H

(11) Zhao, X., *et al*., Mixed-node metal–organic frameworks as efficient electrocatalysts for oxygen evolution reaction. *ACS Energy Letters*, **2018**, *3* (10), p. 2520–2526. https://doi.org/10.1021/acsenergylett.8b01540

(12) Xu, D., *et al*., Flexible quasi-solid-state sodium-ion capacitors developed using 2D metal-organic framework array as reactor. *Advanced Energy Materials*, **2018**, *8* (13), p. 1702769. (https://doi.org/10.1002/aenm.201702769)

(13) Zha, Q., *et al*., Chlorine-doped α-Co (OH) 2 hollow nano-dodecahedrons prepared by a ZIF-67 self-sacrificing template route and enhanced OER catalytic activity. *Dalton Transactions*, **2019**, *48* (32), p. 12127–12136. https://doi.org/10.1039/C9DT02141H

(14) Chen, G., *et al*., Cobalt-based metal–organic framework nanoarrays as bifunctional oxygen electrocatalysts for rechargeable Zn-Air batteries. *Chemistry–A European Journal*, **2018**, *24* (69), p. 18413–18418. https://doi.org/10.1002/chem.201804339

(15) Yang, J., *et al*., Layered structural co-based MOF with conductive network frames as a new supercapacitor electrode. *Chemistry–A European Journal*, **2017**, *23* (3), p. 631–636. https://doi.org/10.1002/chem.201804339

(16) Abdelkader-Fernandez, V. K., *et al*., Noble-metal-free MOF-74-derived nanocarbons: insights on metal composition and doping effects on the electrocatalytic activity toward oxygen reactions. *ACS Applied Energy Materials*, **2019**, *2* (3), p. 1854–1867. https://doi.org/10.1021/acsaem.8b02010

(17) Madhu, R., *et al*., Recent developments in transition metal-based MOFs for electrocatalytic water splitting emphasizing fundamental and structural aspects. *Materials Chemistry Frontiers*, **2023**. *7* (11), p. 2120–2152. https://doi.org/10.1039/D3QM00089C

(18) Han, Y., *et al*., Direct carbonization of cobalt-doped NH 2-MIL-53 (Fe) for electrocatalysis of oxygen evolution reaction. *Nanoscale*, **2016**. *8* (2), p. 1033–1039. https://doi.org/10.1039/C5NR06626C

(19) Li, Y., *et al*., 2D metal–organic-framework array-derived hierarchical network architecture of cobalt oxide flakes with tunable oxygen vacancies towards efficient oxygen evolution reaction. *Journal of Catalysis*, **2018**. *364*, p. 48–56. https://doi.org/10.1016/j.jcat.2018.05.006

(20) Wang, Y. Z., *et al*., Recent advances in complex hollow electrocatalysts for water splitting. *Advanced Functional Materials*, **2022**. *32* (6), p. 2108681. https://doi.org/10.1002/adfm.202108681

(21) Dinh, K. N., *et al*., Ultrathin porous NiFeV ternary layer hydroxide nanosheets as a highly efficient bifunctional electrocatalyst for overall water splitting. *Small*, **2018**, *14* (8), p. 1703257. https://doi.org/10.1002/smll.201703257

(22) Maity, K., *et al*., Co(II)-doped Cd-MOF as an efficient water oxidation catalyst: doubly interpenetrated boron nitride network with the encapsulation of free ligand containing pyridine moieties. *ACS Applied Materials & Interfaces*, **2017**, *9* (43), p. 37548–37553. https://doi.org/10.1021/acsami.7b12926

(23) Wang, Y., *et al*., Electrode modification and optimization in air-cathode single-chamber microbial fuel cells. *International Journal of Environmental Research and Public Health*, **2018**, *15* (7), p. 1349. https://doi.org/10.3390/ijerph15071349

(24) Keim, W., *Catalysis in C1 Chemistry*. Vol. 4. 2012: Springer Science & Business Media. https://link.springer.com/book/10.1007/978-94-009-7040-3

(25) De Villenoisy, T., *et al*., Principles of design and synthesis of metal derivatives from MOFs. *Advanced Materials*, **2023**, *35* (24), p. 2210166. https://doi.org/10.1002/adma.202210166

(26) Yuan, K., *et al*., Boosting oxygen reduction of single iron active sites via geometric and electronic engineering: nitrogen and phosphorus dual coordination. *Journal of the American Chemical Society*, **2020**, *142* (5), p. 2404–2412. https://doi.org/10.1021/jacs.9b11852

(27) Wang, Q., *et al*., In situ growth of Fe (ii)-MOF-74 nanoarrays on nickel foam as an efficient electrocatalytic electrode for water oxidation: a mechanistic study on valence engineering. *Chemical Communications*, **2019**, *55* (75), p. 11307–11310. https://doi.org/10.1039/C9CC05087F

(28) Xing, J., *et al*., In situ growth of well-ordered NiFe-MOF-74 on Ni foam by Fe 2+ induction as an efficient and stable electrocatalyst for water oxidation. *Chemical communications*, **2018**, *54* (51), p. 7046–7049. https://doi.org/10.1039/C8CC03112F

(29) Connor, P., *et al*., The determination of electrochemical active surface area and specific capacity revisited for the system MnOx as an oxygen evolution catalyst. *Zeitschrift für Physikalische Chemie*, **2020**, *234* (5), p. 979–994. https://doi.org/10.1515/zpch-2019-1514

(30) Matyushov, D. V., Standard electrode potential, Tafel equation, and the solvation thermodynamics. *The Journal of Chemical Physics*, **2009**, *130* (23). https://doi.org/10.1063/1.3152847

(31) Chahal S; Bandyopadhyay A.; Dash, S. P.; Kumar P., Microwave synthesized 2D gold and its 2D-2D hybrids. *J. Phys Chem Lett*. **2022**, *13*, 6487–95. https://doi.org/10.1021/acs.jpclett.2c01540

(32) Krishtalik, L. I., *Charge Transfer Reactions in Electrochemical and Chemical Processes*. 2012, Springer Science & Business Media. https://link.springer.com/book/10.1007/978-1-4684-8718-3

(33) Saleh, F. S. and Easton, E. B., Determining electrochemically active surface area in PEM fuel cell electrodes with electrochemical impedance spectroscopy and its application to catalyst durability. *Electrochimica Acta*, **2013**. *114*, p. 278-284. https://doi.org/10.1016/j.electacta.2013.10.050